Biosensors and Bioelectronics 131 (2019) 214–223

Contents lists available at ScienceDirect

Biosensors and Bioelectronics

journal homepage: www.elsevier.com/locate/bios

Graphene oxide and gold nanoparticle based dual platform with short DNA probe for the PCR free DNA biosensing using surface-enhanced Raman scattering

Ibrahim Khalil[a], Wageeh A. Yehye[a,*], Nurhidayatullaili Muhd Julkapli[a], Shahrooz Rahmati[a], Abu Ali Ibn Sina[b], Wan Jefrey Basirun[a,c], Mohd Rafie Johan[a]

[a] Nanotechnology & Catalysis Research Centre (NANOCAT), Institute of Graduate Studies, University of Malaya, Kuala Lumpur 50603, Malaysia
[b] Centre for Personalised Nanomedicine, Australian Institute for Bioengineering and Nanotechnology (AIBN), The University of Queensland, Corner of College and Cooper Roads (Bldg 75), Brisbane QLD 4072, Australia
[c] Department of Chemistry, Faculty of Science, University of Malaya, Kuala Lumpur 50603, Malaysia

ARTICLE INFO

Keywords:
Graphene oxide-gold nanoparticles
Surface-enhanced Raman scattering
DNA biosensor
Sandwich biosensor
Short-length DNA probe
Malayan box turtle

ABSTRACT

Surface-enhanced Raman scattering (SERS) based DNA biosensors have considered as excellent, fast and ultrasensitive sensing technique which relies on the fingerprinting ability to produce molecule specific distinct spectra. Unlike conventional fluorescence based strategies SERS provides narrow spectral bandwidths, fluorescence quenching and multiplexing ability, and fitting attribute with short length probe DNA sequences. Herein, we report a novel and PCR free SERS based DNA detection strategy involving dual platforms and short DNA probes for the detection of endangered species, Malayan box turtle (MBT) (*Cuora amboinensis*). In this biosensing feature, the detection is based on the covalent linking of the two platforms involving graphene oxide-gold nanoparticles (GO-AuNPs) functionalized with capture probe 1 and gold nanoparticles (AuNPs) modified with capture probe 2 and Raman dye (Cy3) via hybridization with the corresponding target sequences. Coupling of the two platforms generates locally enhanced electromagnetic field 'hot spot', formed at the junctions and interstitial crevices of the nanostructures and consequently provide significant amplification of the SERS signal. Therefore, employing the two SERS active substrates and short-length probe DNA sequences, we have managed to improve the sensitivity of the biosensors to achieve a lowest limit of detection (LOD) as low as 10 fM. Furthermore, the fabricated biosensor exhibited sensitivity even for single nucleotide base-mismatch in the target DNA as well as showed excellent performance to discriminate closely related six non-target DNA sequences. Although the developed SERS biosensor would be an attractive platform for the authentication of MBT from diverse samples including forensic and/or archaeological specimens, it could have universal application for detecting gene specific biomarkers for many diseases including cancer.

1. Introduction

DNA sensing technology has rapidly emerged since last decades to get the biological footprints of every species. Current technologies for DNA identification such as sequencing, microarray and mass spectrometry are labor-intensive, time-consuming and require expensive equipment. In addition, the use of short length DNA probe in the widely accepted PCR based techniques (e.g. sequencing) for the DNA biosensing is often very challenging (Ngo et al., 2016). While short-length amplicons, typically ≤150 bp in length improve the better recovery of the detection from the degraded DNA specimens or compromised forensic evidence (Turna et al., 2010), reduction of amplicon length in PCR based technique is limited by low specificity, producing artifacts in the final results (Ali et al., 2012; Hird et al., 2006). Therefore, nanoparticles based DNA sensing has recently considered as one of the best alternatives to the conventional strategies to conserve the high specificity and sensitivity using very short segment of DNA as the detection probe (Merkoçi, 2010). In recent years, nanoparticles based DNA biosensors are employed in diversified applications including identification of pathogenic microorganisms (Tondro et al., 2018), detection of cancer biomarkers (Huang et al., 2018; Shahrokhian and Salimian, 2018), trace elements, environmental hazards, drug screening, and the analysis of gene sequences (Li et al., 2005; Saidur et al., 2017) and food safety (Ha et al., 2017). Thus we believe that nanoparticle based DNA

* Corresponding author.
E-mail address: wdabdoub@um.edu.my (W.A. Yehye).

https://doi.org/10.1016/j.bios.2019.02.028
Received 27 August 2018; Received in revised form 14 January 2019; Accepted 3 February 2019
Available online 19 February 2019
0956-5663/

sensing technology (e.g. SERS) could be strategic to identify the endangered species such as Malayan box turtle (MBT). MBT is an endangered and vulnerable turtle species but an attractive item to the illegal wildlife trader due to its huge appeal as an exotic food item and in traditional medicine. Moreover, MBT is a natural scavenger of waste materials, hence carrier of several pathogenic microorganisms, parasites, various toxins, and heavy metals (Ali et al., 2016; Green et al., 2010). Therefore, consumption of or contact with this turtle and/or turtle-derived materials in food chains and medicines have significant health concerns which urge for the reliable authentication technique for this turtle species to restrict health hazards, as well as to prevent or reduce illegal trades.

SERS has emerged as the most powerful analytical technique for the fast and ultra-sensitive detection of DNA with single molecule differentiations by providing intrinsic chemical information and vibrational fingerprints of each molecules (Nie and Emory, 1997; Xu et al., 2015). It has certain advantages over fluorescence, spectroscopic, electrochemistry and some other techniques. For instance, no photo-bleaching from the Raman tags or Raman scattering compound, availability of large number of Raman labels which have broaden up the scope to select the right label according to the experimental design applications, unique spectral fingerprint from the Raman tag upon laser excitation and the narrow spectrum peak widths that opens up the opportunity of high level multiplex detection (Kneipp et al., 2006; Zhang et al., 2010). SERS phenomenon can be explained by the two enhancement mechanisms, the electromagnetic and the chemical or charge transfer mechanisms. Electromagnetic enhancement is due to the enhanced electromagnetic fields localized to few nanometers of a nanostructured metallic surface formed by surface plasmon resonances while chemical enhancement results from the resonant charge transfer effects between the metal and the molecule that is strongly chemically adsorbed onto its surface (Khalil et al., 2016; Maher, 2012). However, nanoparticle-based SERS signaling is mostly dependent on the highly localized regions of intense local field 'hot spots' which is formed in the nanoscale junctions and interstitial crevices of the two or more interacting SERS substrates and consequently provide extraordinary enhancements of up to 10^{15} orders of magnitude to the SERS signal (Hao and Schatz, 2004; Qian et al., 2008). Therefore, metallic nanostructures in different forms such as nanoparticles, nanorod, nanogaps, nanoshells, nanostars, dimers, and many more as well as combination of different materials were utilized to explore the hot spots and employed in DNA sensing as it could greatly increase the Raman cross section of the immobilized biomolecules, leading to a low detection limit (Khalil et al., 2016; Lu et al., 2011). GO-AuNP hybrid composites have recently been proved as an effective SERS platforms due to the synergistic effect of two individual components which can magnify the weak Raman signals (Khalil et al., 2016). However, the integration of GO-AuNP hybrid composites with AuNPs has never been explored which we believe can further enhance the Raman signal of the adsorbed molecules with many order of magnitude via electromagnetic and chemical enhancement in comparison to the individual components (either GO, AuNPs or GO-AuNP hybrid alone). Thus, DNA sensing strategy that uses both GO-AuNP hybrid composite and AuNPs as the sensor platforms, could revolutionize the current biosensing techniques for detecting endangered species as well as DNA biomarkers for many diseases including cancer.

Herein we develop a novel and PCR free SERS DNA biosensor which utilizes a sandwich platform comprising of GO-AuNPs hybrid for target capture and SERS tagged AuNPs for target detection. The hybridization of target sequence with the capture and detection probe facilitates the covalent agglomeration of the strongly coupled plasmonic AuNPs over GO-AuNPs and thereby exhibits locally enhanced electromagnetic field at the junction. The use of dual platforms thus significantly enhanced the SERS signal due to the 'hot spot' generation between GO-AuNPs and AuNPs system (Hao and Schatz, 2004; He et al., 2012; Qian et al., 2008). The developed platform detects target DNA sequence of endangered MBT species, using a short length DNA capture probe which is a limitation for current PCR based techniques. In our study, the Raman tag was attached directly onto the AuNPs surfaces which minimizes the distance dependent limitations, and produced intense SERS spectra by the charge transfer mechanism between the Cy3 and AuNP surfaces (Wabuyele and Vo-Dinh, 2005). With this greater amplification of the SERS signal generated by the sandwich duplex structure, a detection limit of as low as 10 fM is achieved. Moreover, our dual platform shows excellent sequence specificity and sensitivity to discriminate single-base mismatches. In comparison with other SERS DNA biosensors, our fabricated sandwich biosensor is cost effective and avoids complex manipulation of ssDNA probe without intercalating the Raman tags. We believe that this simple but highly selective, specific and sensitive DNA sensing approach would be useful for wide-range of biosensing applications.

2. Materials and methods

2.1. Chemicals and instruments

Gold chloride trihydrate ($HAuCl_4{\cdot}3H_2O$), sodium citrate dihydrate ($C_6H_5Na_3O_7{\cdot}2H_2O$) (≥99%), graphite powder (< 20 μm), tris(2-carboxyethyl) phosphine hydrochloride (≥98%) (TCEP) and Tris-EDTA (TE) buffer solution, pH 7.4 were obtained from Sigma Aldrich. Potassium permanganate ($KMnO_4$), phosphoric acid (H_3PO_4) were purchased from R & M Chemicals Ltd.; sulphuric acid (H_2SO_4) (95–97%), hydrochloric acid (HCl) (37%), and ethanol (99.8%) from Friendemann Schmidt and hydrogen peroxide (H_2O_2) (35%) from Quality Reagent Chemical (Qrec). DPEC treated water was purchased from Biobasic Canada Inc. while ultrapure water (UPW) (18.2 MΩ cm) was prepared from CASCADA LS Water, Pall UltraPure Water System and used throughout the study. The rest of the chemicals were of analytical reagent grade and used as per requirement.

Washing and purification of the GO, AuNP and GO-AuNPs were done by using high speed Heraeus Multifuge X3FR Centrifuge, Thermo Scientific. On the contrary, Mini-15K CE High Speed Mini Centrifuge was employed throughout the study for the washing of unbound DNA, washing or separation of nanoparticles/nanocomposites. Ultrasonic homogenizer (TF-650Y) was used for the exfoliation of GO. UV–vis experiments were conducted by using UV-2600 UV–vis spectrophotometer (Shimadzu co., Ltd, Japan). High resolution Transmission electron microscopy (HRTEM) was performed using lacy carbon coated copper grid with FEI Tecnai F20 TWIN 200 kV transmission electron microscope (FEI company, Hillsboro, USA). X-ray diffraction (XRD) was performed by using PANalytical X-ray diffractometer (model EMPYREAN, Almelo, Netherlands). SERS spectra were recorded using Renishaw Invia Confocal Raman Microscope. Atomic Force Microscopy (AFM) was performed using AFM5000II Scanning Probe Microscope (Hitachi) in dynamic force (tapping) mode.

2.2. Probe, target and non-target DNAs

The probe DNA sequence (31-mer) was selected from the short length DNA fragment (120 bp) of mitochondrial cytochrome b (cytb) gene of MBT species. The sequence was developed and verified by PCR technique for the detection of MBT species from complex food matrices by Ali et al. (2016). As a sensing strategy, the probe DNA sequence was designed to split into two fractions – 16-mer and 15-mer length which were further modified with 5′ thiol modifier with 6-carbon spacer arm and 3′ thiol modifier with 3-carbon spacer arm respectively. All the oligonucleotide sequences (listed in Table 1) were synthesized and purified by the Integrated DNA Technologies (IDT), Singapore. The lyophilized oligonucleotides were resuspended in TE buffer (10 mM Tris HCl, 1 mM EDTA, pH 7.4) as per manufacturer instructions and kept at −40 °C as stock solution in 100 μM concentration. To prepare the working standard or dilution from the stock solution, DPEC treated water was used throughout the study.

Table 1
List of oligonucleotide sequences.

Name	Sequence profile
Capture probe 1 (16-mer) (CP1)	: SH-$(CH_2)_6$-5′-GAT-CAT-TAC-TAG-GCA-C 3′
Capture probe 2 (15-mer) (CP2)	: 5′CTG-CCT-AAT-CCT-TCA 3′-$(CH_2)_3$-SH
Target DNA	: 5′TGA-AGG-ATT-AGG-CAG-GTG-CCT-AGT-AAT-GAT-C3′
Non-complementary DNA	: 5′CAG-GAA-GCC-GAA-TGA-ACA-TTC-GAC-GGC-AGC-T3′
Non-target DNA (Buffalo)	: 5′TGC-AGG-ATT-AGG-CAG-ATG-CCT-AGG-AGA-GAG-C3′
Non-target DNA (Horse)	: 5′TGG-AGG-ATT-AGG-CAG-ATT-CCT-AGG-AGG-GAG-C3′
Non-target DNA (Cow)	: 5′TGT-AGG-ATT-AGG-CAG-ATT-CCC-AGG-AGG-GAA-C3′
Non-target DNA (Pork)	: 5′AGG-GCG-GTA-ATG-ATG-AAT-GGC-AGG3′
Non-target DNA (Dog)	: 5′TGG-CTG-TGT-CCG-ATG-TAT-AGT-GCA-AGT-CCA-CTT3'
One-base mismatch DNA	: 5′TGA-AGG-ATT-AGG-CAA-GTG-CCT-AGT-AAT-GAT-C3′
Three-base mismatch DNA	: 5′TGA-AGG-ATT-AGG-TGA-GTG-CCT-AGT-AAT-GAT-C3′

2.3. Synthesis of GO, AuNPs and GO-AuNP nanocomposites

GO and AuNPs were synthesized as per protocol described by Marcano et al. (2010) and Liu and Lu (2006) respectively with few modifications and described in details at Supporting information (Section 1.1 and 1.2). GO-AuNPs composites were synthesized by the citrate reduction of gold (III) salt as per reported procedure with minor modifications (Goncalves et al., 2009). An aqueous suspension of GO (0.5 mg/mL, 20 mL) was prepared by ultrasonication for 2 h, followed by the addition of syringe filtered 100 mL $HAuCl_4{\cdot}3H_2O$ solution (1 mM). The resultant suspension was then aged for 30 min with continuous stirring to promote the interaction of Au ions with GO surface. The suspension was then heated until 80 °C and 2 mL of $C_6H_5Na_3O_7{\cdot}2H_2O$ (300 mmol) aqueous solution was added promptly into it. The reaction was continued at 80 °C with stirring for another 4 h. The resulting GO-AuNPs composite was centrifuged at 6000 RPM for 2 h and washed three times with UPW to eliminate the free AuNPs. The final GO-AuNPs nanocomposite was resuspended in UPW and stored in the refrigerator.

2.4. Attachment of thiol-modified capture probe DNA to AuNPs and GO-AuNPs

To activate the thiol-modified oligo DNA, 100 μL of 1 mM CP1 and CP2 were treated separately with 10 μL of freshly prepared 10 mM TCEP and incubated at room temperature (RT) for 1 h. Thiol-activated single-stranded (ss) oligonucleotide was then bound to the AuNPs and GO-AuNPs following the procedure developed by Sun et al. (2007) with little modifications. As-prepared AuNPs (3 mL) and GO-AuNPs (500 μL) suspension into two different Eppendorf tubes were centrifuged at 8000 RPM for 30 min and the pellets were re-dispersed with 0.1 mM PBS (pH 7.4) to produce final volume 300 μL and 500 μL respectively. TCEP treated CP1 was added into GO-AuNPs while CP2 into AuNPs tube, mixed well with gentle hand shaking and incubated for 16 h at RT in dark environment. After 16 h, 10 mM PBS (pH 7.4) with 0.1% Tween 20 was added to the mixture to result in a solution with a final buffer concentration of 1 mM PBS with 0.01% Tween 20 and kept standing for 30 min. Next, the salt aging of the DNA functionalized nanoparticles was initiated slowly with 1 M NaCl to reach the final NaCl concentration of 100 mM. NaCl was added gradually at an interval of 1 h and the increment rate was such that after first addition of 1 M NaCl it reached to 10 mM. At each NaCl increment, a certain amount of DNA is attached, allowing the AuNPs and GO-AuNPs to survive the next small increment of salt. Moreover, the conformation of DNA is also changed from being parallel to an upright arrangement on the AuNP surface which provides more effective steric stability as well as make easy availability of DNA sequences for further hybridization (Cutler et al., 2012; Zhang et al., 2013). The samples were further allowed to age under the same conditions for another 40 h at RT. The aged solution was then centrifuged at 8000 RPM for 20 min and pipetted off the supernatant as much as possible to remove the free DNA. Functionalized nanoparticles were again dispersed in washing buffer (0.1 mM PBS and 100 mM NaCl, pH 7.4) and centrifuged at 8000 RPM for 20 min and the procedure was repeated for 2–3 times. Finally, GO-AuNP immobilized CP1 (GO-AuNP-CP1) precipitates were dispersed in 0.1 mM PBS (pH 7.4) and 100 mM NaCl buffer and stored at refrigerator for further use.

2.5. Attachment of Cy3-cysteamine to oligo-functionalized AuNPs

Thiolated Cy3 (1000 μL, 1 μM) was treated with 100 μL of freshly prepared 10 mM TCEP and incubated for 1 h at RT. TCEP treated Cy3 was added to the red oily precipitate of AuNP-CP2, obtained from the previous step and allowed to keep for 24 h with frequent manual stirring. The solution was then centrifuged at 8000 RPM for 20 min and the supernatant was discarded. The precipitate was washed with nanopure water by successive centrifugation and redispersion in nanopure water. It has already been established that formation of monolayer of ssDNA after attachment of thiolated DNA onto AuNPs, there were still spaces on AuNPs surface for the subsequent attachment of Raman tags (Sun et al., 2007).

2.6. Fabrication of GO-AuNPs DNA biosensor

GO-AuNP-CP1 (400 μL) was incubated with corresponding target DNA (100 μL) for overnight at RT. GO-AuNP-CP1-Target nanocomposite was centrifuged at 8000 RPM for 20 min and washed twice with washing buffer to remove the unhybridized target DNA. The GO-AuNP-CP1-Target nanocomposite was then dispersed into nanopure water for the subsequent hybridization with equal quantity of AuNP-DNA2-Cy3 in the microcentrifuge tube, shaken manually and incubated at RT for overnight to facilitate the hybridization of the CP2 with the unbound part of the target DNA. The hybridized compound (GO-AuNP-CP1-Target-CP2-AuNP-Cy3) was centrifuged at low speed (4000 RPM for 5 min) and washed several times with washing buffer to remove the unbound AuNP-DNA2-Cy3. The final nanocomposite was dispersed into nanopure water, followed by the preparation of corresponding slide for SERS experiment by dropping 50 μL each of the sample on the silicon wafer. The sample spot was dried under vacuum created using vacuum pump at ambient condition and SERS spectra were acquired using Renishaw Invia Confocal Raman Microscope with a 20× working objective lens. The sample was excited by using 532 nm laser with 5-mW power at the laser source with 50 μm diameter spot. All of the obtained Raman spectra were chopped to reveal Raman bands with/without applicable baseline correction. All these manipulations were conducted using the Origin Pro 9.1 software.

3. Results and discussion

3.1. Design and principle of the biosensor

The principle of dual platform based (i.e. GO-AuNPs and AuNPs) SERS detection of DNA is illustrated in Fig. 1. We employed a

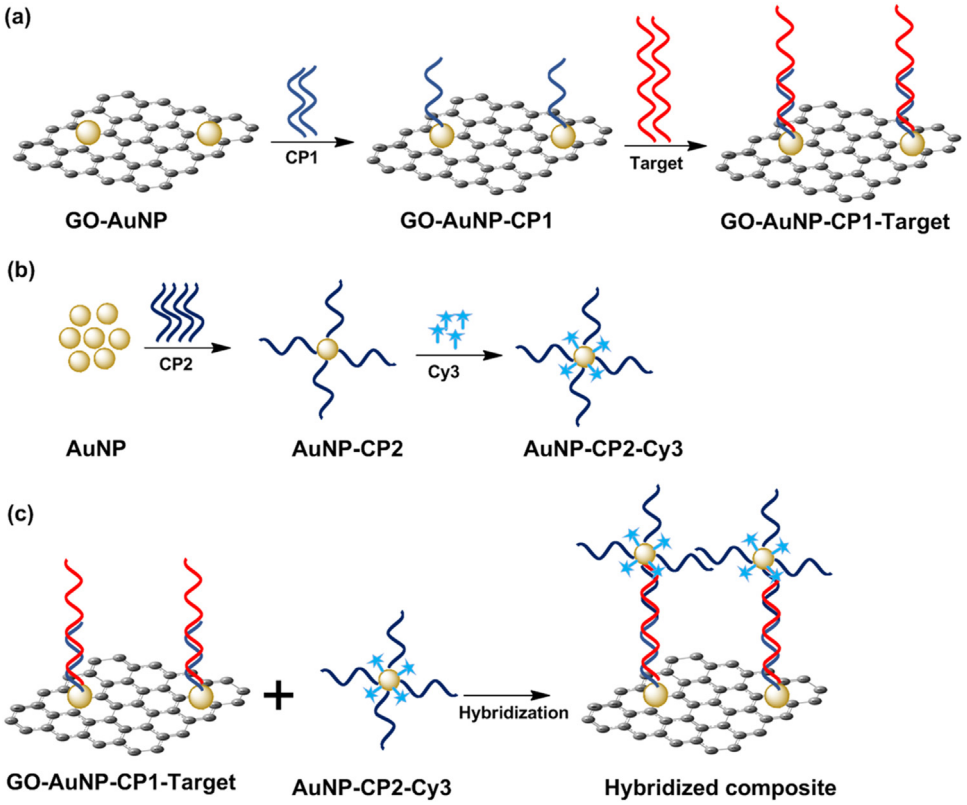

Fig. 1. The schematic illustration of SERS sandwich biosensor based on GO-AuNPs and AuNPs dual platforms.

'sandwich' assay strategy which involves attachment of CP1 on GO-AuNPs composites by the well-established Au-S bonding followed by hybridization with corresponding target sequences (Fig. 1a). On the other hand, CP2 was immobilized onto another platform (i.e. AuNPs) followed by the attachment of Cy3 Raman tag (Fig. 1b). The covalently bound Raman Tags which are in close proximity to the AuNPs surface ensure strong SERS signals to be observed (Sun et al., 2007). CP1 and CP2 are thiolated at the 5′ and 3′ end respectively which allows facile self-assembly of DNA strands on AuNP surfaces through formation of Au–S bonds (Zhang et al., 2007). In between thiol group and nucleotide bases of the capture probes (CP1 and CP2) we have added 6-carbon spacer to keep the capture probes in upright conformation and free for hybridization as DNA bases in proximity of AuNPs could face difficulties due to steric effect at the surfaces (Park et al., 2002; Zhang et al., 2007). In the construction of SERS biosensor (Fig. 1c), a sandwich complex was formed via a binary networking between the two platforms upon mixing together where CP2 immobilized on AuNPs were hybridized with the remainder target sequence attached to GO-AuNPs (Mucic et al., 1998; Sun et al., 2007). The SERS signal finally confirms the presence of target DNA sequence in the dual platform.

3.2. Characterization of GO, AuNPs, and GO-AuNPs nanocomposite

The XRD spectra of GO showed a dominant diffraction peak at 2θ = 10.65° corresponding to an interlayer spacing is 8.30 Å (Fig. S1a), indicating that the starting graphite flakes had been oxidized to GO (Marcano et al., 2010). XRD analysis of the synthesized AuNPs represents the five peaks at 2θ = 38.19° (d-spacing: 2.35 Å), 44.38° (2.04 Å), 56.68° (1.62 Å), 64.70° (1.44 Å) and 77.67° (1.22 Å) (Fig. S1a), corresponding to the Reference code 96-901-1614 of HighScore Plus library, and standard Bragg reflections (crystal planes) of (111), (200), (200), (220), and (311) of Au face centers cubic (fcc) lattice. The intense peak at 56.68° represents the preferential growth in the (200) direction. The GO-AuNP composites also showed the four major peaks at 38.10° (d-spacig: 2.36 Å), 44.30° (2.04 Å), 64.70° (1.44 Å) and 77.64° (1.22 Å) confirming the presence of AuNPs on the GO (Fig. S1a) (Pocklanova et al., 2016).

The characteristic UV spectrum of GO exhibited a major peak at 232 nm, corresponding to the plasmonic π→π* transitions (C=C bonds) (Fig. S1b) (Heuer-Jungemann et al., 2015). The as prepared AuNP solution was burgundy red in color and reflected an absorption band at 520 nm in the visible spectrum (Fig. S1b) (Goncalves et al., 2009). The anticipated shape and diameter of AuNPs are spherical and 13 nm in average which in consequent justified by the HR-TEM examination (Fig. 2b), hence comply the previous study (Liu and Lu, 2006). GO-AuNPs hybrids showed two peaks at 240 and 522 nm, representing the characteristic absorption of GO and AuNPs respectively, as well as dictating the successful attachment of AuNPs over GO (Fig. S1b) (Zhang et al., 2012). The result is consistent with HR-TEM (Fig. 2c). The synthesized GO was also characterized by the Raman spectra comprising G-band at 1600 cm^{-1} and D-band at 1350 cm^{-1} whereas GO-AuNP composite was characterized by a moderate blue shift (4 cm^{-1}) as the D-band shifted from 1350 cm^{-1} to 1346 cm^{-1} (Fig. S1c). This shift suggests an interaction between AuNPs and GO substrate and ensures AuNPs were deposited on GO (Subrahmanyam et al., 2010). More importantly, there was a significant increase of Raman spectra for GO-AuNPs in compare to GO (~2.5 times higher of G-band value), implies the obvious effect of AuNPs in the synthesized GO-AuNPs which might be due to the electromagnetic SERS enhancement (He et al., 2012; Li et al., 2016).

3.3. Attachment of capture probe DNAs and Raman Tag to nanoparticles

The conjugation of 15-mer long ssDNA to AuNPs converted the pristine ruby red AuNPs solution to a pinkish-red solution and this relative reduction of the color density is due to the reduced amount of free AuNPs (Thavanathan et al., 2014). After the attachment of thiolated DNA on AuNPs, the UV–Vis spectra showed a peak shifting from 520 to 524 nm, which is due to the increase of AuNPs size through

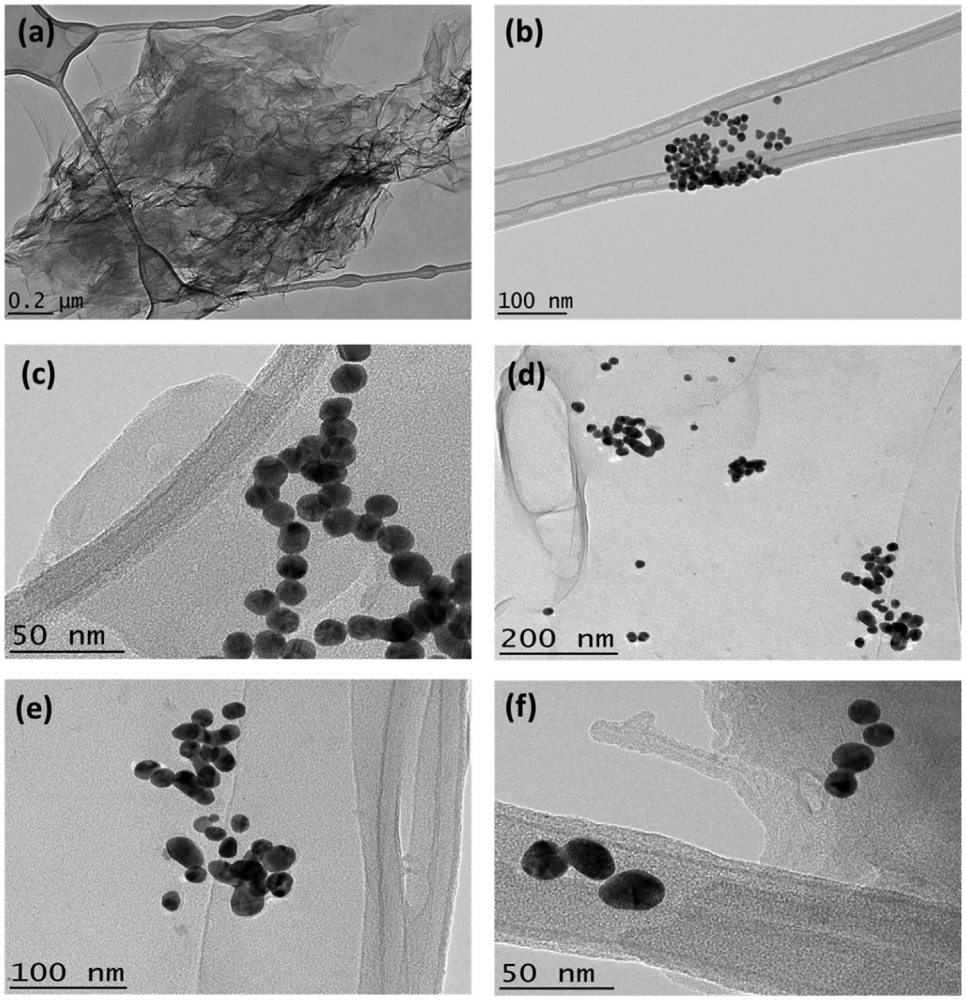

Fig. 2. HR-TEM images of (a) GO, (b) AuNP and (c) GO-AuNP on lacy carbon coated copper grid. (d–f) HR-TEM images of hybridized composites via the coupling of two platforms, GO-AuNPs and AuNPs via the hybridization of the capture probe sequences with the complementary target sequence. As hybridization happened, AuNPs were found mostly aggregated or linked to each other on GO sheets.

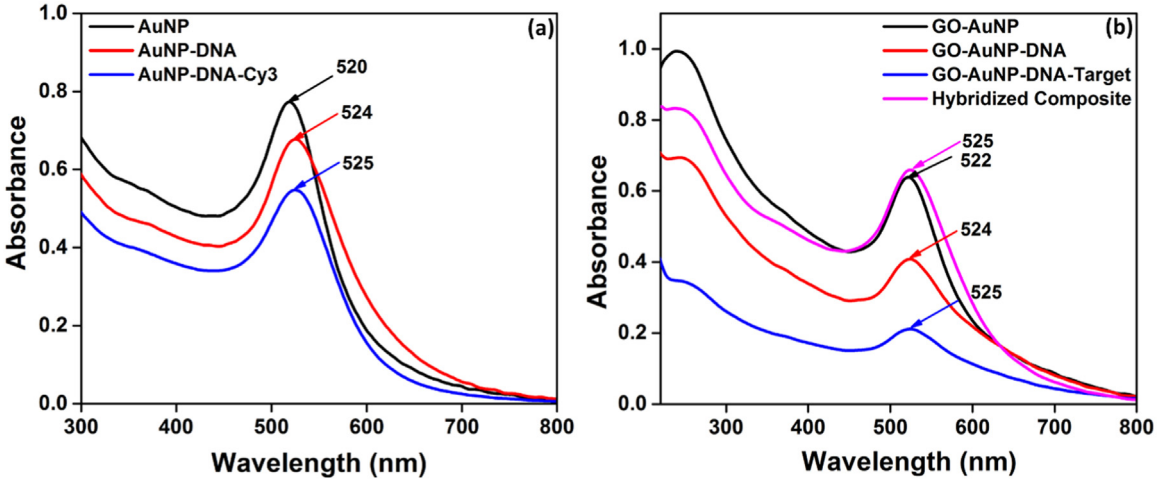

Fig. 3. UV–vis absorption spectra of (a) AuNP, AuNPs-ssDNA and AuNP-ssDNA-Cy3 and (b) GO-AuNPs, GO-AuNPs modified with thiolated CP2, followed by corresponding Target and finally the hybridized composite.

conjugation with DNA probe, suggesting the successful binding of ssDNA to the AuNPs. Addition of thiolated Cy3 to AuNP-DNA composite, there was a slight red shifting (1 nm) of the peak at 525 nm, indicating further increase of the AuNPs size, and confirms the attachment of Cy3 on AuNP-DNA composites (Fig. 3a) (Thavanathan et al., 2014). Similarly, absorption spectrum of GO-AuNPs hybrids functionalized with ss-CP1 showed AuNPs characteristic peak shifting from 522 nm to 524 nm (Fig. 3b), confirming the immobilization of

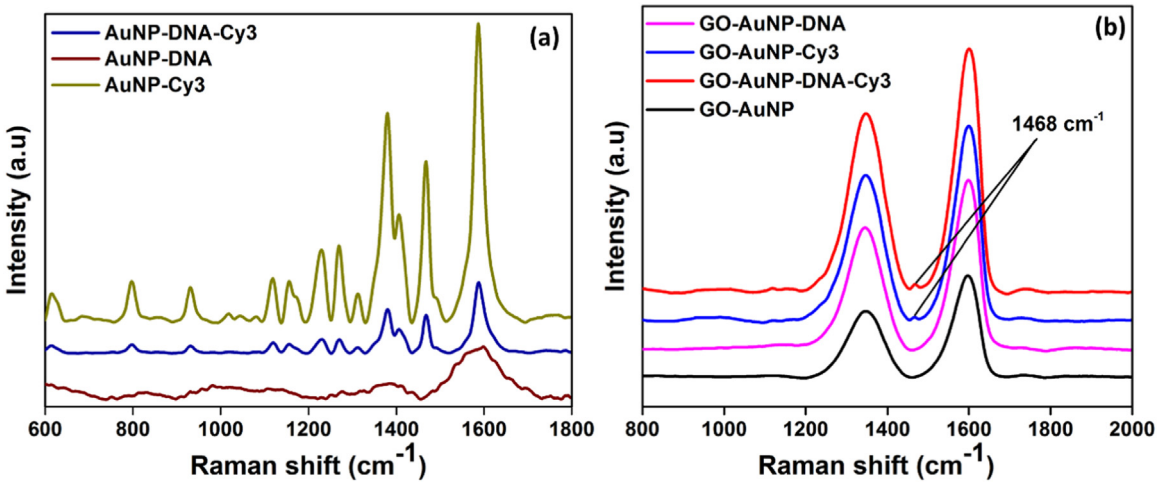

Fig. 4. Raman spectra of AuNPs functionalized with DNA, Cy3 and both DNA and Cy3 (a) GO-AuNP and GO-AuNP functionalized with DNA, Cy3 and both DNA and Cy3 (b).

thiolated probe DNA over GO-AuNPs (Wang et al., 2016). However, Atomic Force Microscopy (AFM) study of AuNPs-DNA indicated the well dispersion of AuNPs (Fig. S2a–d) which may be due to the electrostatic repulsion between AuNPs for oligo functionalization (Csaki et al., 2001). AFM images of GO-AuNPs before and after DNA functionalization also justified well distribution of AuNPs on GO sheets (Fig. S2e–h). Moreover, it also demonstrated that AuNPs and GO-AuNPs are stable at gradual increment of NaCl (1 M) during DNA salt-aging process which thus ensures smooth hybridization process.

3.4. Justification of the biosensing strategy

AuNPs were functionalized with CP2 as well as further modified with thiolated Raman dye by Au-S linkage and considered as signal probes. Raman spectra of AuNPs-Cy3 reflected the exact fingerprints of Cy3 dye which is characterized by the peaks predominantly at 616, 798, 937, 1121, 1158, 1233, 1270, 1384, 1470, and 1592 cm^{-1} (Fig. 4a). Immobilization of Cy3 onto AuNPs produced the spectral fingerprint with greater enhancement of Raman scattering which is due to the combined effect of electromagnetic enhancement and charge transfer mechanism (Jans and Huo, 2012). However, the incorporation of ss probe DNA to form the composite, AuNPs-CP2-Cy3, had no influence over the Cy3 fingerprint spectra but a decreased intensity. This reduced intensity is proportional to the less immobilized Cy3 which might be due to prior attachment of ss probe DNA to AuNPs (Fig. 4a). Therefore, to demonstrate the feasibility of the signal control, a Cy3 concentration optimization study was conducted and described in the Supporting information. The unique features in the signal probe design is that Raman tag was not incorporated in the probe DNA rather directly immobilized onto AuNPs via strong Au-S covalent bonding. Thus avoided complex manipulation in the probe sequences and keeping the ss-probe sequence completely free for hybridization with corresponding target sequences, which made the process robust (Sun et al., 2007).

The CP1 was immobilized on SERS active GO-AuNPs nanocomposites by Au-S bonding and used as the detection probes subsequently. Attachment of CP1 onto GO-AuNPs followed by hybridization with corresponding target sequences was confirmed by UV–Vis spectra with broadened red-shifted plasmon band (Fig. 3b) (Storhoff et al., 2000). This widening of the peak might be due to the increasing of the particle size formed by the GO-AuNPs-CP1-Target composite. The hybridization of GO-AuNPs-CP1-Target with CP2-AuNP-Cy3 can be explained by the red shift in the particle surface plasmon resonance from 520 to 525 nm, and wide broadening of the peak with greater intensity at 525 nm position which might be due to attachment of more AuNPs composites with the existing GO-AuNPs by the corresponding probe sequences against the target DNA (Fig. 3b) (Mucic et al., 1998; Storhoff et al., 2000). Moreover, to justify the hybridization process by SERS, GO-AuNPs platform was functionalized with Cy3 both in the absence and presence of ss probe DNA. Only a single peak representing the Cy3 at 1468 cm^{-1} is distinguishable and visible as the other major peaks of Cy3 are overlapped by D and G band of GO (Fig. 4b) (Prinz et al., 2016). Therefore, as expected the hybridized composites were also found to produce the SERS peak at 1468 cm^{-1} representing the Cy3 attached with AuNPs as well as G-band at 1355 cm^{-1} and D-band at 1590 cm^{-1} characteristic to GO (Fig. S3), ensuring the linking of the two platforms via the covalent attachment of the probes and corresponding target.

HR-TEM images of the hybridized products also justify that AuNPs are linked with each other in maximum cases which indicates the successful hybridization was happened between the two strands of the CP sequences via complementary target sequences (Fig. 2d–f). However, few single AuNPs also found over the GO sheets, indicating no hybridization happened which might be due to the lack of either strand of the DNA probe sequences or somehow could not find the complementary sequences to be hybridized. Moreover, to justify the hybridization event happened throughout the reaction systems as well as to validate the preparation of the slide for SERS study, a repeatability study of a hybridized composite was conducted by taking SERS spectra from the randomly selected three different locations of the same slide (Fig. S5a). The error of the SERS peak at 1468 cm^{-1} for the three different locations varied only very little with acceptable linearity (R^2 = 0.94) (Fig. S5b).

3.5. Analytical performance of the biosensor

3.5.1. Selectivity of the biosensor

The specificity of the biosensor was solely dependent on the covalent linking of the both platforms via hybridization of split probe sequences with corresponding target DNA and the appearance of representative Cy3 and GO peaks from the SERS spectra. Detection of MBT target sequence is indicated by the presence of D and G band of GO along with peak at 1468 cm^{-1} position as Cy3 signatory peak. However, due to the use of short DNA probes in our approach, there is a possibility of having similar nucleotide sequence in the whole genome sequence of other species than MBT. Thus, to check the similarity in sequence, the selectivity of the probe and non-target DNA sequences was justified theoretically. The uniqueness of the 31-mer probe DNA sequence was checked by multiple aligning with cytb gene of MBT and 27 other meat and fish species (Table S1) using MEGA5 alignment tool (http://www.megasoftware.net/) which revealed 100% matching only with MBT and scored 6–15 nucleotide (19.4–48.4%) mismatching with

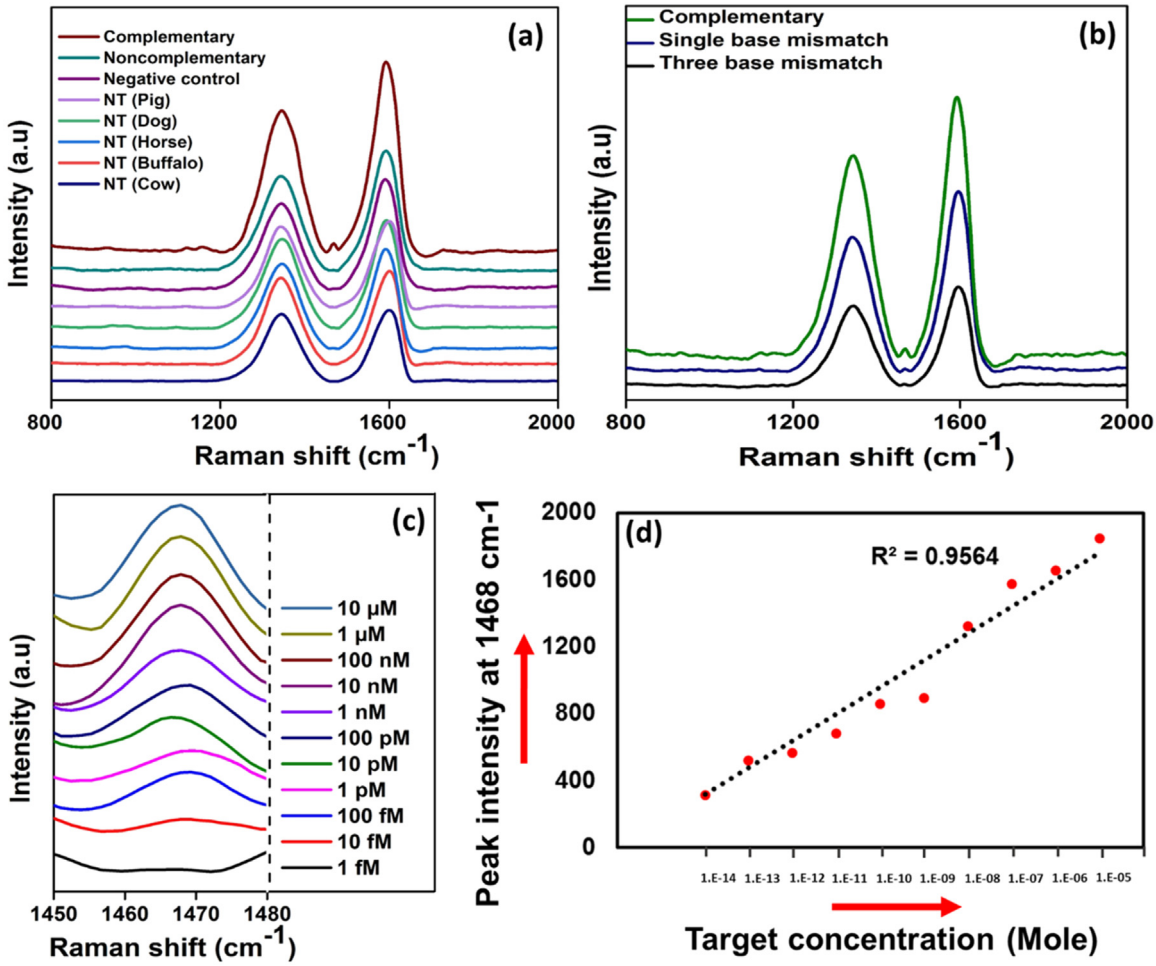

Fig. 5. (a) SERS spectra of the selectivity study. DNA hybridization containing complementary, non-complementary, negative control (blank) and non-Target sequences (pig, dog, horse, buffalo, and cow), and (b) SERS spectra of the biosensor hybridized with corresponding (red), single-base mismatch (dark blue) and three-base mismatches (black) target sequences. (c) Stacked SERS spectra of Cy3 peak at 1468 cm^{-1} of the composites hybridized with varying concentration of MBT target DNAs (10 µM to 1 fM), displayed from the upper to the lower direction. Here, the spectra were chopped into 1450–1480 cm^{-1} to magnify and distinguish the intensity at peak 1468 cm^{-1}. (d) Linear plot of SERS intensities of 1468 cm^{-1} band versus corresponding target DNA concentration.

other non-target species (Table S1), therefore reflecting huge genetic distance and unlikelihood of cross-species recognition in a real experiment. In our experiments, the selectivity of the biosensor was evaluated following different control hybridization reactions accomplished by the presence and absence of target DNA sequences and the replacement of target sequence with non-complementary DNA sequences. In detail, substitution of the target sequence was done by i) 31-mer long oligonucleotide sequence with 100% mismatch nucleotide bases, ii) complementary target sequence of the three non-target species (buffalo, horse and cow) having the 6–8 mismatches (Table S1), and iii) two other non-target sequences with distinct length – pork (24-mer) and dog (33-mer). In the presence of the corresponding target sequence, GO-AuNP-CP1-Target-CP2-AuNP-Cy3 sandwich composite was formed by the coupling of the two platforms, generates the SERS hot spot and consequently strong SERS signal characterized by Cy3 fingerprint peak at 1468 cm^{-1} along with GO representing G and D band (Fig. 5a). This SERS spectra therefore indicates a true positive result (Chuong et al., 2017). On the other hand, SERS spectra from the control samples such as hybridized composite with no target sequence (blank sample) generated only GO representing peaks without any existence of Cy3 spectral fingerprint (Fig. 5a), therefore, suggesting no hybridization event due to lack of bridging target sequences. Therefore, the peak intensity at 1468 cm^{-1} for the blank sample is being considered as the baseline signal for Cy3 and the obtained spectra is denoted as the true negative.

The SERS spectra of the hybridized composite achieved in the presence of non-complementary (100% mismatch) and complementary target sequences of the non-target species (cow, buffalo, horse, dog and pig) however, revealed representing GO peaks and in rare cases with very little existence of Cy3 signal (Fig. 5a). The presence of this very weak Cy3 signal could be considered as false positive, and the intensity is ignored in this study due to the equal or lower signal-to-noise ratio. This little existence of Cy3 spectra might be due to some nonspecific interaction between the fabricated GO-AuNPs-CP1-T and AuNPs-CP2-Cy3 composites, however could not produce intense Cy3 SERS signal due to lack of hot-spot generation. This is because hot spots are generally originated at the interstices between adjacent AuNPs rather than between GO sheet and AuNPs (Chuong et al., 2017). Moreover, due to the dominant presence of the D and G band of GO, all other less intense Cy3 peaks were also minimized (Prinz et al., 2016). A true positive signal is therefore distinguishable from the false positive by the distinct Cy3 fingerprint peak at 1468 cm^{-1}. Therefore, the results showed that the fabricated sensor is highly efficient to distinguish target and non-target DNA sequences of the closely related species and suggesting no hybridization event between the capture probes and complementary target sequence of the non-target species. The selectivity experiment thus confirms the theoretical finding that the probe is highly specific for MBT species only and there is no chance for the hybridization with non-target species.

3.5.2. Sensitivity of the biosensor

The efficiency of biosensor in terms of the ability to distinguish the corresponding target sequences bearing single-base mismatch and three-base mismatches were tested. As shown in Fig. 5b, the hybridized composite via the base-mismatch target sequence generated SERS spectra (i.e. Cy3 representative peak at 1468 cm^{-1}) at lower intensity in comparison to the fully complementary sequence. This is attributed to the fact that mismatched DNA might undergo irregular attachment with the complementary probe sequences due to the base changes in the sequence. The data in Fig. 5b thus indicates that the higher the number of base mismatches in the sequence, the lower the SERS intensity due to the irregular hybridization. This data clearly suggests that the developed biosensor is sensitive enough to distinguish the DNA with single nucleotide variation. We believe that one of the main reasons behind this greater efficiency is probably the use of very short fragment of ss DNA (only 15 and 16 bases long) as the probe sequences for detecting target DNA.

3.5.3. Dynamic detection range of the biosensor

Quantitative detection of the target sequence was performed by measuring the SERS intensity of the representative signal probe - Cy3 from the hybridized compounds formed via the varying concentration of target DNA. Each Target sample is ten times diluted from its previous concentration to provide a series of target DNA concentration from 10 μM to 1 fM. The SERS intensity was in downward trend with the decreasing concentration of the target DNA from 10 μM to 10 fM (Fig. S6 and Fig. 5c). However, there was no/almost indistinguishable Cy3 signal from the hybridized composite for the target concentration below 10 fM. The SERS spectra were background (baseline) corrected, and a standard curve for the intensity of the Cy3 peak at 1468 cm^{-1} position versus target concentrations was plotted (Fig. 5d). An R^2 value of 0.96 was obtained from the linear regression analysis of the peak height at 1468 cm^{-1} against the corresponding target DNA concentration. This data suggests that our biosensor can be applicable in detecting target DNA sequence from a wide range of sample concentration. This greater sensitivity of our fabricated biosensor relied on few aspects such as using GO-AuNPs as the SERS platform where maximum number of AuNPs were being deposited over the large planer surface of GO which in consequent facilitated the covalent binding of CP1 sequences in greater numbers, hence creating more options even for the minute quantity of the target sequences to be hybridized. Even if single CP2 bound to AuNP-Cy3 hybridize with the corresponding unbound portion of target sequence, the Cy3 signal would be strong due to more Cy3 molecules bound over the same AuNP-CP2 composite (Fig. 1c). Moreover, covalent linking of the detection and signal probe via hybridization event brings the two platforms within few nanometer ranges, therefore generates hotspots at the junction of GO-AuNPs and AuNPs which in consequent lead to strong highly localized enhancement of SERS signal. In addition to the electromagnetic, a minor enhancement due to the resonant charge transfer process between the AuNPs and Cy3 is also contributed to the detected Raman signal. This chemical enhancement might be due to the vibrationally excited state of the adsorbed Cy3 molecule which is caused by two ways - either by exciting electrons from AuNPs to unoccupied molecular orbitals of adsorbed Cy3 and back to the AuNPs or electrons from the occupied molecular orbitals into the Fermi level of AuNPs and back to the adsorbed molecule (Maher, 2012; Radziuk and Moehwald, 2015). Hence to justify the contribution of the hot spots in signal enhancement, SERS spectra of hybridized sandwich composite in absence of Cy3 was compared to bare GO-AuNPs and the enhancement is about 26% more intense than GO-AuNPs (Fig. S7). This enhancement is definitely due to the agglomeration of AuNPs over GO-AuNPs via hybridization and hot spot generated at the junctions between AuNPs rather than AuNPs deposition over GO sheet (Chuong et al., 2017). Moreover, functionalization of AuNPs-CP2 with Cy3, followed by hybridization and coupling with GO-AuNPs-CP1-T, enhances SERS signals 15% (Fig. S7) more than the hybridized composite without Cy3, therefore, dictates the contribution of chemical enhancement by the adsorbed Cy3 molecule.

The use of SERS active dual nanoparticle platforms, and short length oligo marker, made our biosensor viable and amenable for the detection of trace amount of DNA (e.g. LOD is 10 fM) present in the sample. The fabricated biosensor showed better capability to detect MBT species in comparison to the some of the PCR based detection techniques involving 120 base pair long amplicon by conventional PCR, PCR-RFLP and SYBR green real-time PCR techniques (Ali et al., 2015, 2016; Asing et al., 2016). Hence, the detection principle will be efficient enough for the unambiguous tracing of MBT materials in the food chain, or any forensic or archaeological investigations and tracking of trafficking. Moreover, SERS biosensors exhibited better sensitivity than the biosensors fabricated by single platform using Raman label at the terminal end of reporter DNA (He et al., 2012) and even using the dual platforms following sandwich assay procedure (Kang et al., 2010; Zhang et al., 2010). Some of the sandwich assay procedure involved SERS non-active platform hence required further step such as exfoliation of a graphene layer over the hybridized composite (Prinz et al., 2016) or silver enhancement of the hybridized composites (Cao et al., 2002). Therefore, to address the shortcomings as well as to make the sensing way easy, flawless, and convenient, we have employed two different SERS active platforms and only few simple steps involvement to produce multicomponent aggregates upon hybridization to get greater SERS intensity via the localized hot spots. Furthermore, Cy3 was directly immobilized onto the AuNPs which also directly contributed on the total enhancement by the charge transfer mechanisms. Finally, we believe that using different SERS active substrate and applying the same biosensing principle, it will be possible to establish a multiplex DNA sensor for the detection of multiple DNA biomarker sequences from different origin.

4. Conclusion

We have demonstrated dual platform-based PCR free SERS assay for the efficient and sensitive detection of DNA. To fabricate the device, short probe sequences were immobilized onto two different nanostructure platforms to form GO-AuNPs-CP1 and AuNPs-CP2-Cy3, considered as detection and signal probe respectively. The novel features of the sensor are the use of very short length probe sequences and the linking of the two SERS active platforms via target-probe DNA hybridization to produce a unique and enhanced SERS signal. This huge enhancement is in fact due to the combined effects of electromagnetic enhancement via the hot spot generated by multicomponent assembly as well as the chemical enhancement by the charge transfer mechanism between Cy3 and AuNPs surfaces. Therefore, the presence of target DNA up to 10 fM, was even able to combine the two platforms together to generate the unique and distinguishable SERS spectra. The biosensors thus provide the LOD down to 10 fM and could differentiate the target sequences difference with single nucleotide variation. Furthermore, the fabrication of the biosensor is easy, convenient, involves low-cost SERS substrate and provides extraordinary specificity to discriminate the corresponding sequences of the closely related non-target meat species. The SERS biosensor thus revealed better suitability and efficiency for the detection and quantification of MBT materials in the food chain to remove the ambiguity, hence could be adopted by the regulatory authorities, archaeologists and wildlife protection agencies for the forensic or archaeological authentication even under compromised conditions as well as tracking of the MBT trafficking with greater reliability and confidence. Moreover, this PCR free, short length split-probe DNA conjugated dual platforms based SERS sensing technology will also be suitable for detecting any short length DNA biomarkers. Thus, we believe that this platform could be considered as a model for the detection of life threatening pathogenic microorganisms, cancers, verification of food adulteration, authentication of species, forensic applications and guided us for the multiplex detection.

CRediT authorship contribution statement

Ibrahim Khalil: Conceptualization, Methodology, Formal analysis, Software, Data curation, Validation, Visualization, Writing - original draft. **Wageeh A. Yehye:** Conceptualization, Funding acquisition, Investigation, Project administration, Resources, Supervision, Writing - review & editing. **Nurhidayatullaili Muhd Julkapli:** Investigation, Supervision, Writing - review & editing. **Shahrooz Rahmati:** Conceptualization, Methodology, Visualization, Software. **Abu Ali Ibn Sina:** Writing - review & editing. **Wan Jefrey Basirun:** Funding acquisition, Investigation, Supervision. **Mohd Rafie Johan:** Project administration, Resources.

Acknowledgement

The authors would like to thank Dr. Eaqub Ali and Dr. M.A. Motalib Hossain, University of Malaya for their intellectual support and assistance in providing Lab facility for oligo DNA handling and storage. This work was financially supported by the Grand Challenge project (GC001B-14SBS), Postgraduate Research Grant (PPP) (PG190-2015B) and UMRG programme (RP044C-17AET) of University of Malaya, Malaysia.

Declaration of interests

None.

Appendix A. Supporting information

Supplementary data associated with this article can be found in the online version at https://doi.org/10.1016/j.bios.2019.02.028.

References

Ali, M.E., Asing, Hamid, S.B.A., Razzak, M.A., Rashid, N.R.A., Al Amin, M., Mustafa, S., 2015. A suitable method to detect potential fraud of bringing Malayan box turtle (Cuora amboinensis) meat into the food chain. Food Addit. Contam.: Part A 32 (8), 1223–1233.

Ali, M.E., Hamid, S.B.A., Hossain, M.M., Mustafa, S., Kader, M.A., Zaidul, I., 2016. Lab-on-a-chip-based PCR-RFLP assay for the detection of malayan box turtle (Cuora amboinensis) in the food chain and traditional Chinese medicines. PloS One 11 (10), e0163436.

Ali, M.E., Kashif, M., Uddin, K., Hashim, U., Mustafa, S., Man, Y.B.C., 2012. Species authentication methods in foods and feeds: the present, past, and future of halal forensics. Food Anal. Methods 5 (5), 935–955.

Asing, Ali E., Hamid, S.B.A., Hossain, M., Ahamad, M.N.U., Hossain, S.A., Naquiah, N., Zaidul, I., 2016. Duplex real-time PCR assay using SYBR Green to detect and quantify Malayan box turtle (Cuora amboinensis) materials in meatballs, burgers, frankfurters and traditional Chinese herbal jelly powder. Food Addit. Contam.: Part A 33 (11), 1643–1659.

Cao, Y.C., Jin, R., Mirkin, C.A., 2002. Nanoparticles with Raman spectroscopic fingerprints for DNA and RNA detection. Science 297 (5586), 1536–1540.

Chuong, T.T., Pallaoro, A., Chaves, C.A., Li, Z., Lee, J., Eisenstein, M., Stucky, G.D., Moskovits, M., Soh, H.T., 2017. Dual-reporter SERS-based biomolecular assay with reduced false-positive signals. Proc. Natl. Acad. Sci. USA 114 (34), 9056–9061.

Csaki, A., Möller, R., Straube, W., Köhler, J.M., Fritzsche, W., 2001. DNA monolayer on gold substrates characterized by nanoparticle labeling and scanning force microscopy. 29 (16) (e81-e81).

Cutler, J.I., Auyeung, E., Mirkin, C.A., 2012. Spherical nucleic acids. J. Am. Chem. Soc. 134 (3), 1376–1391.

Goncalves, G., Marques, P.A., Granadeiro, C.M., Nogueira, H.I., Singh, M., Gracio, J., 2009. Surface modification of graphene nanosheets with gold nanoparticles: the role of oxygen moieties at graphene surface on gold nucleation and growth. Chem. Mater. 21 (20), 4796–4802.

Green, A.D., Buhlmann, K.A., Hagen, C., Romanek, C., Gibbons, J.W., 2010. Mercury contamination in turtles and implications for human health. J. Environ. Health 72 (10), 14–23.

Ha, N.-R., Jung, I.-P., La, I.-J., Jung, H.-S., Yoon, M.-Y., 2017. Ultra-sensitive detection of kanamycin for food safety using a reduced graphene oxide-based fluorescent aptasensor. Sci. Rep. 7, 40305.

Hao, E., Schatz, G.C., 2004. Electromagnetic fields around silver nanoparticles and dimers. J. Chem. Phys. 120 (1), 357–366.

He, S., Liu, K.-K., Su, S., Yan, J., Mao, X., Wang, D., He, Y., Li, L.-J., Song, S., Fan, C., 2012. Graphene-based high-efficiency surface-enhanced Raman scattering-active platform for sensitive and multiplex DNA detection. Anal. Chem. 84 (10), 4622–4627.

Heuer-Jungemann, A., Kiessling, L., Stratakis, E., Kymakis, E., El-Sagheer, A.H., Brown, T., Kanaras, A.G., 2015. Programming the assembly of gold nanoparticles on graphene oxide sheets using DNA. J. Mater. Chem. C 3 (36), 9379–9384.

Hird, H., Chisholm, J., Sánchez, A., Hernandez, M., Goodier, R., Schneede, K., Boltz, C., Popping, B., 2006. Effect of heat and pressure processing on DNA fragmentation and implications for the detection of meat using a real-time polymerase chain reaction. Food Addit. Contam. 23 (7), 645–650.

Huang, R., He, N., Li, Z., 2018. Recent progresses in DNA nanostructure-based biosensors for detection of tumor markers. Biosens. Bioelectron. 109, 27–34.

Jans, H., Huo, Q., 2012. Gold nanoparticle-enabled biological and chemical detection and analysis. Chem. Soc. Rev. 41 (7), 2849–2866.

Kang, T., Yoo, S.M., Yoon, I., Lee, S.Y., Kim, B., 2010. Patterned multiplex pathogen DNA detection by Au particle-on-wire SERS sensor. Nano Lett. 10 (4), 1189–1193.

Khalil, I., Julkapli, N.M., Yehye, W.A., Basirun, W.J., Bhargava, S.K., 2016. Graphene–gold nanoparticles hybrid—synthesis, functionalization, and application in a electrochemical and surface-enhanced raman scattering biosensor. Materials 9 (6), 406.

Kneipp, K., Kneipp, H., Bohr, H.G., 2006. Single-molecule SERS spectroscopy. Surface-Enhanced Raman Scattering. Springer, pp. 261–277.

Li, Y., Cu, Y.T.H., Luo, D., 2005. Multiplexed detection of pathogen DNA with DNA-based fluorescence nanobarcodes. Nat. Biotechnol. 23 (7), 885–889.

Li, Y., Yang, J., Zhou, Y.-Z., Zhong, T., Zheng, S.-H., Zeng, W.-W., 2016. Facile synthesis of gold nanoparticles-graphene oxide films and their excellent surface-enhanced Raman scattering activity. Mon. Chem.-Chem. Mon. 147 (4), 677–683.

Liu, J., Lu, Y., 2006. Preparation of aptamer-linked gold nanoparticle purple aggregates for colorimetric sensing of analytes. Nat. Protoc. 1 (1), 246.

Lu, G., Li, H., Liusman, C., Yin, Z., Wu, S., Zhang, H., 2011. Surface enhanced Raman scattering of Ag or Au nanoparticle-decorated reduced graphene oxide for detection of aromatic molecules. Chem. Sci. 2 (9), 1817–1821.

Maher, R.C., 2012. SERS hot spots. In: Kumar, C.S.S.R. (Ed.), Raman Spectroscopy for Nanomaterials Characterization. Springer Berlin Heidelberg, Berlin, Heidelberg, pp. 215–260.

Marcano, D.C., Kosynkin, D.V., Berlin, J.M., Sinitskii, A., Sun, Z., Slesarev, A., Alemany, L.B., Lu, W., Tour, J.M., 2010. Improved synthesis of graphene oxide. ACS Nano 4 (8), 4806–4814.

Merkoçi, A., 2010. Nanoparticles-based strategies for DNA, protein and cell sensors. Biosens. Bioelectron. 26 (4), 1164–1177.

Mucic, R.C., Storhoff, J.J., Mirkin, C.A., Letsinger, R.L., 1998. DNA-directed synthesis of binary nanoparticle network materials. J. Am. Chem. Soc. 120 (48), 12674–12675.

Ngo, H.T., Wang, H.-N., Fales, A.M., Vo-Dinh, T., 2016. Plasmonic SERS biosensing nanochips for DNA detection. Anal. Bioanal. Chem. 408 (7), 1773–1781.

Nie, S., Emory, S.R., 1997. Probing single molecules and single nanoparticles by surface-enhanced Raman scattering. Science 275 (5303), 1102–1106.

Park, S.-J., Taton, T.A., Mirkin, C.A., 2002. Array-based electrical detection of DNA with nanoparticle probes. Science 295 (5559), 1503–1506.

Pocklanova, R., Rathi, A.K., Gawande, M.B., Datta, K.K.R., Ranc, V., Cepe, K., Petr, M., Varma, R.S., Kvitek, L., Zboril, R., 2016. Gold nanoparticle-decorated graphene oxide: synthesis and application in oxidation reactions under benign conditions. J. Mol. Catal. A: Chem. 424, 121–127.

Prinz, J., Matković, A., Pešić, J., Gajić, R., Bald, I., 2016. Hybrid structures for surface-enhanced raman scattering: dna origami/gold nanoparticle dimer/graphene. Small 12 (39), 5458–5467.

Qian, X., Zhou, X., Nie, S., 2008. Surface-enhanced Raman nanoparticle beacons based on bioconjugated gold nanocrystals and long range plasmonic coupling. J. Am. Chem. Soc. 130 (45), 14934–14935.

Radziuk, D., Moehwald, H., 2015. Prospects for plasmonic hot spots in single molecule SERS towards the chemical imaging of live cells. Phys. Chem. Chem. Phys. 17 (33), 21072–21093.

Saidur, M.R., Aziz, A.R.A., Basirun, W.J., 2017. Recent advances in DNA-based electrochemical biosensors for heavy metal ion detection: a review. Biosens. Bioelectron. 90, 125–139.

Shahrokhian, S., Salimian, R., 2018. Ultrasensitive detection of cancer biomarkers using conducting polymer/electrochemically reduced graphene oxide-based biosensor: application toward BRCA1 sensing. Sens. Actuators B: Chem. 266, 160–169.

Storhoff, J.J., Lazarides, A.A., Mucic, R.C., Mirkin, C.A., Letsinger, R.L., Schatz, G.C., 2000. What controls the optical properties of DNA-linked gold nanoparticle assemblies? J. Am. Chem. Soc. 122 (19), 4640–4650.

Subrahmanyam, K.S., Manna, A.K., Pati, S.K., Rao, C.N.R., 2010. A study of graphene decorated with metal nanoparticles. Chem. Phys. Lett. 497 (1), 70–75.

Sun, L., Yu, C., Irudayaraj, J., 2007. Surface-enhanced Raman scattering based non-fluorescent probe for multiplex DNA detection. Anal. Chem. 79 (11), 3981–3988.

Thavanathan, J., Huang, N.M., Thong, K.L., 2014. Colorimetric detection of DNA hybridization based on a dual platform of gold nanoparticles and graphene oxide. Biosens. Bioelectron. 55, 91–98.

Tondro, G., Vais, R.D., Sattarahmady, N., 2018. An optical genosensor for Enterococcus faecalis using conjugated gold nanoparticles-rRNA oligonucleotide. Sens. Actuators B: Chem. 263, 36–42.

Turna, J., Marcela, B., Domenico, P., 2010. Polymerase chain reaction–restriction fragment length polymorphism (PCR-RFLP) as a molecular discrimination tool for raw and heat-treated game and domestic animal meats. J. Food Nutr. Res. 49 (3), 134–139.

Wabuyele, M.B., Vo-Dinh, T., 2005. Detection of human immunodeficiency virus type 1 DNA sequence using plasmonics nanoprobes. Anal. Chem. 77 (23), 7810–7815.

Wang, Q., Li, Q., Yang, X., Wang, K., Du, S., Zhang, H., Nie, Y., 2016. Graphene oxide–gold nanoparticles hybrids-based surface plasmon resonance for sensitive

detection of microRNA. Biosens. Bioelectron. 77, 1001–1007.
Xu, L.-J., Lei, Z.-C., Li, J., Zong, C., Yang, C.J., Ren, B., 2015. Label-free surface-enhanced Raman spectroscopy detection of DNA with single-base sensitivity. J. Am. Chem. Soc. 137 (15), 5149–5154.
Zhang, H., Harpster, M.H., Park, H.J., Johnson, P.A., Wilson, W.C., 2010. Surface-enhanced Raman scattering detection of DNA derived from the West Nile virus genome using magnetic capture of Raman-active gold nanoparticles. Anal. Chem. 83 (1), 254–260.
Zhang, J., Song, S., Wang, L., Pan, D., Fan, C., 2007. A gold nanoparticle-based chronocoulometric DNA sensor for amplified detection of DNA. Nat. Protoc. 2 (11), 2888–2895.
Zhang, Q., Ren, Q., Miao, Y., Yuan, J., Wang, K., Li, F., Han, D., Niu, L., 2012. One-step synthesis of graphene/polyallylamine–Au nanocomposites and their electrocatalysis toward oxygen reduction. Talanta 89, 391–395.
Zhang, X., Gouriye, T., Go¨eken, K., Servos, M.R., Gill, R., Liu, J., 2013. Toward fast and quantitative modification of large gold nanoparticles by thiolated DNA: scaling of nanoscale forces, kinetics, and the need for thiol reduction. J. Phys. Chem. C 117 (30), 15677–15684.